NATO ADVANCED STUDY INSTITUTE

on

OPTICS IN ASTROPHYSICS

ASTRONOMICAL SPECKLE INTERFEROMETRY

Review lecture by Y.Balega from the
Special Astrophysical Observatory, Zelentchuk, Russia
(preliminary version)

Institut d'etudes scientifiques de Cargese, 2002

CONTENTS:

1. Introduction

Everybody knows that telescopes make things bigger: the bigger the telescope the more there is to see. However, atmospheric turbulence limits angular resolution to about 1 arcsec; consequently, a 10-m telescope has approximately the same resolving capabilities as a small 10-cm diameter tube. Resolution limitations caused by the atmospheric smearing, were first overcame by Michelson and his collaborators in 1920s by making use of interferometric properties of light. As you all know, they succeeded to measure the angular diameter of the red supergiant star Betelgeuse using the 5 m baseline installed at the 100-inch telescope. Similar methods have been later used extensively in radio astronomy and in the optical intensity interferometry to reach an angular resolution of 0.001 arcsec and better.

Labeyrie (1970) first pointed out that very short exposure photographs contain information on scales at the telescope diffraction limit. In the 70s the technique called speckle interferometry became one of the most promising developments in the optical observational astronomy. It became an extremely active field scientifically with important contributions made to a wide range of topics in stellar astrophysics. Here

we will make a short review of the speckle interferometry and present the most important results obtained by astronomers using this method at large telescopes.

2. Speckle phenomena

The short-exposure image of a point source formed by a corrugated wave front is composed of numerous short-lived speckles. Speckles result from the interference of light from many coherent patches, of typical diameter r_0, distributed over the full aperture of the telescope. J.Texereau (1963) was one of the first who described correctly the speckle phenomena in his study of limitations of the image quality in large telescopes. He observed boiling light granules visually using a strong eye-piece and by means of sensitive photographic films in the focus of the 1.93m telescope at Haute-Provence. Earlier, visual observers of binary stars, such as W.Finsen, could use the speckle structure of a binary star image to yield useful information about the separations and position angles between the components. In this manner they have been used the speckle interferometry method without knowing about it.

A single r_0-size subpupil would form a PSF of width $\sim\lambda / r_0$ imposed by diffraction. Diffraction pattern produced by a circular aperture is called the Airy spot. It is made of a very bright central spot surrounded by rings, which are alternately dark and bright. The radius of the first dark ring of the diffraction spot is equal to:

$$\alpha = 1.22\ \lambda / D$$

We now consider two small-size subpupils, separated by a distance $\sim d$, pierced into an opaque screen in front of the telescope aperture. Each small opening diffracts the incoming light, which is spread over the focal plane. The observed phenomena of a modulation pattern of linear interference fringes, is known as Young ‘s fringes. These are normal to the line joining the two subpupils, and the distance that separates a dark from a bright fringe (fringe width) is $\sim \lambda / d$.

Atmospheric turbulence causes random phase fluctuations of the incoming optical wave front. As a result of the randomly varying phase difference between the two subpupils, the fringe pattern moves by a random amount. Phase fluctuations are equivalent to wave front tilts if the assumed subpupils are smaller than r_0. In typical

atmospheric conditions, these fluctuations become uncorrelated when the baseline d exceeds about 10 cm. When the phase shift between the subpupils is equal or greater than the fringe spacing λ / d, fringes will disappear in a long exposure. Instead of making a long exposure, one can follow their motion by recording a sequence of short exposures, short enough to "freeze" the instantaneous fringe pattern.

Now let us introduce a third small subpupil in front of the telescope, which is not collinear with the former two (fig.1). The result will be the pattern of three intersecting moving fringe systems produced by three nonredundant pairs of subpupils. When these fringes interfere, an enhanced bright speckles of width $\sim \lambda / d$ appear.

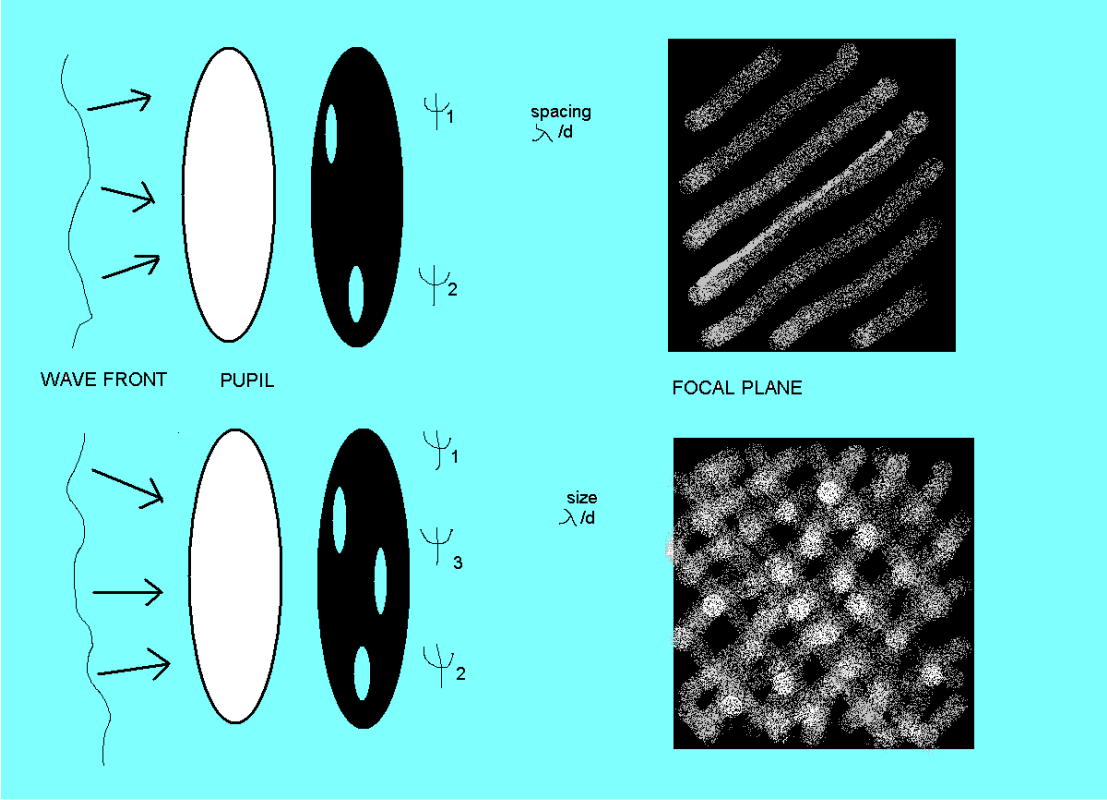

Fig.1. Speckle pattern formation.

The number of speckles N_s per image is defined by the ratio of the area occupied by the seeing disk $\sim \lambda / r_0$ to the area of a single speckle

$$N_s = (\lambda / r_0)^2 \ : \ (\lambda / D)^2 = (D / r_0)^2 \ .$$

If the atmospheric seeing is good, this corresponds to about 1500 speckles in a single short exposure image taken with an 8-m telescope. More accurate estimates give three times less amount of speckles because of the filling factor $k = 0.342$.

(Insert Fig.2 “Speckle image from the 6-m telescope”)

The speckle lifetime τ is defined by the velocity dispersion $\Delta\upsilon$ in the turbulent atmosphere:

$$\tau \sim r_0 / \Delta\upsilon \, .$$

Under typical atmospheric conditions, speckle boiling can be frozen with exposures in the range 0.01 – 0.05 sec.

3. Object-image relation and the Fried parameter

If the atmospheric degradations are isoplanatic all over the telescope field of view, the irradiance distribution from the object $o(x)$ is related to the long-exposure (ensemble averaged) observed irradiance distribution $< i(x) >$ by a convolution relation

$$< i(x) > = o(x) \otimes < s(x) >$$

where the point spread function $< s(x) >$ is simply the long-exposure image of a point source.
In Fourier space it becomes

$$< I(u) > = O(u) \cdot < S(u) >$$

where $< S(u) >$ is the optical transfer function of the system “telescope plus atmosphere”, and u is the spatial frequency vector expressed in radian $^{-1}$. For long exposures, $< S(u) >$ is the product of the transfer function of the telescope $T(u)$ with

the atmospheric transfer function equal to the coherence function $B(u)$ (Roddier 1981):

$$< S(u) > = T(u) \cdot B(u) .$$

Similar to the bandwidth in radio electronics, Fried (1966) proposed to define the resolving power of the telescope as the integral of the optical transfer function:

$$R = \int < S(u) > du = \int T(u) \cdot B(u)\, du .$$

For a large diameter telescope the resolving power depends only upon turbulence and

$$R = \int B(u)\, du.$$

The Fried parameter r_0 has a meaning of the critical telescope diameter for which

$$\int B(u)\, du = \int T(u)\, du,$$

Resolving power of the telescope is limited by the telescope only if $D < r_0$, in other cases it is limited by the atmosphere.
The relation between atmospheric coherence function and r_0 is expressed by:

$$B(u) = exp\ -3.44\ (\lambda u / r_0)^{-5/3}$$ (Fried 1966).

Finally, the following two relations show the dependence of r_0 upon the refraction index structure constant Cn (from the Obukhov's law: the structure function $Dn(\rho) = Cn^2\ \rho^{2/3}$ (Tatarski 1961)) and the wavelength λ :

$$r_0 = [0.423\ k^2\ (\cos z)^{-1} \int\ Cn^2(h)\, dh,$$

$$r_0 \sim \lambda^{6/5} ,$$

here $k = 2\pi / \lambda$, and z is the zenith distance.

4. Labeyrie's method

In the case of short exposures, the image intensity distribution *i(x)* is again related to the object distribution *o(x)* by a convolution relation

$$i(x) = o(x) \otimes s(x) .$$

The Fourier transform of this intensity recording is

$$I(u) = O(u) \cdot S(u),$$

and $$| I(u) |^2 = | O(u) |^2 \cdot | S(u) |^2,$$

here $| O(u) |^2$ is the object power spectrum and $| S(u) |^2$ is the energy spectrum of a point source image. $| S(u) |^2$ describes how the spectral components of the image were transmitted by the atmosphere and the telescope. At every moment this function is not known but its time-averaged value can be determined if the seeing conditions do not change. Time averaging means that

$$<| I(u) |^2> = | O(u) |^2 \cdot <| S(u) |^2>$$

which leads to

$$| O(u) |^2 = <| I(u) |^2> / <| S(u) |^2>.$$

Eq. … gives the essence of the Labeyrie's (1970) proposal, namely: if the time-averaged speckle transfer function is determined from the ensemble of its instant recordings, the intensity of the object's Fourier transform can be reconstructed (see Fig.3). Note that the short-exposure $<| S(u) |^2>$ is not the same as $< S(u) >$ in eq.(…). It includes the high spatial frequency component, which extends, as it was shown both theoretically and from observations, up to the diffraction cut-off limit of the telescope.

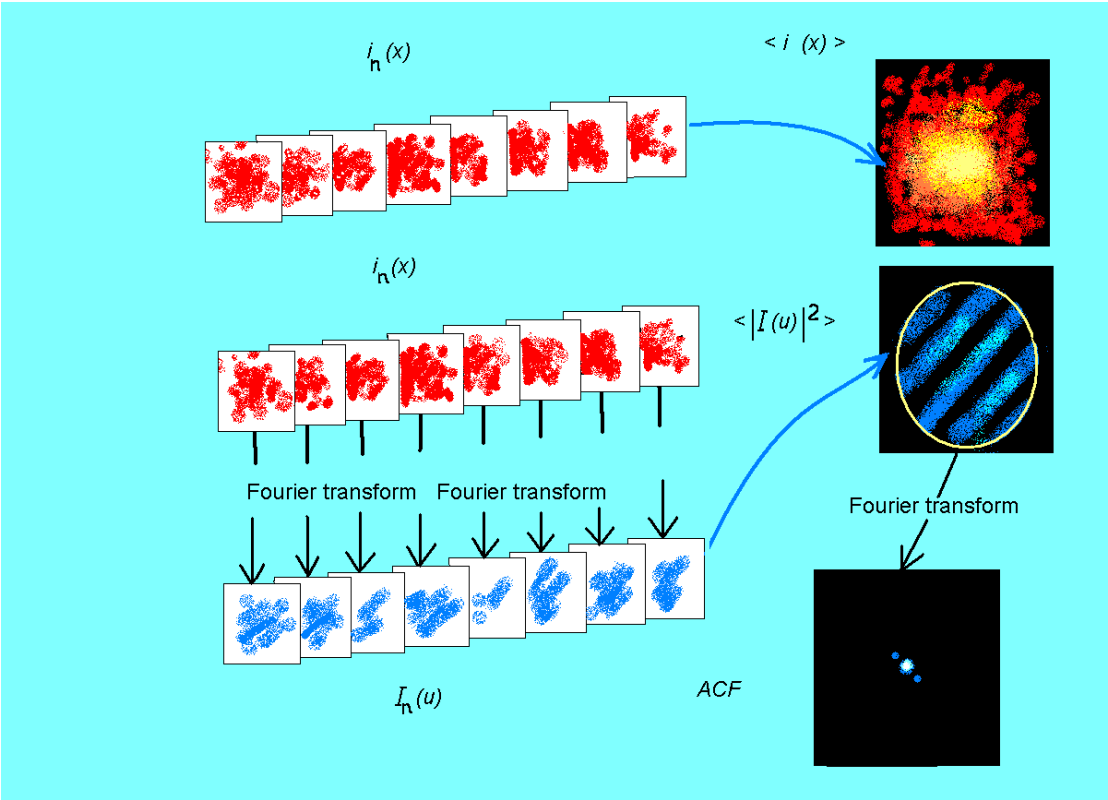

Fig.3. Labeyrie's speckle interferometry.

Analytical expression for the power spectrum of short-exposure images was first proposed by Korff (1973). Its asymptotic behavior is presented in Fig.2, showing that $<|S(u)|^2>$ extends up to the ideal telescope diffraction cut-off frequency. That means that the typical speckle size is of the order of the Airy pattern of the given aperture. The low-frequency part of $<|S(u)|^2>$ corresponds to a long exposure image with the wave front tilts compensated.

Fig.3 explains the difference between the long-exposure image acquisition and the Labeyrie's reconstruction in the case of close binary star observations. A long-exposure photograph of an object is equivalent to adding together or averaging many short photographs. The long-exposure transfer function is not diffraction limited and the result is a very blurred image. In speckle interferometry, the turbulent noise is averaged by composition a large number of short-exposure images.

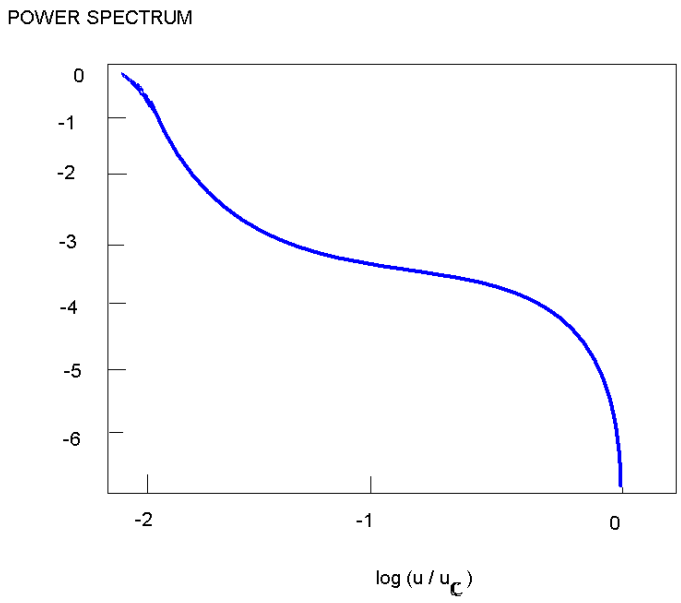

Fig.4. Speckle interferometry transfer function.

It is also convenient to illustrate the Labeyrie's speckle technique in the simple case of an equal magnitudes double star with an angular separation between the components less than the seeing disk of $\sim \lambda / r_0$ size. In this case the image represents a superposition of two identical speckle patterns; vectors, which connect individual speckles from the two components, are equal to the projected position of the stars on the sky (fig.5). High-angular resolution information cannot be extracted from such

Insert Fig.5. "Binary star image reconstruction by speckle interferometry"

blurred images visually, however the binary star can be studied from its Fourier transform pattern or from its averaged autocorrelation

$$< \int i\,(x)\; i\,(x + x')\; dx >$$

which is the inverse Fourier transform of the image power spectrum.

An important consideration for narrow-angle speckle interferometry is the sky coverage defined by the isoplanatic patch (see the lecture of C.Paterson).

5. Speckle interferometry technology: cameras, detectors, photon noise, photon-counting hole.

The ideal speckle camera should satisfy the following two conditions:

- high-resolution short-exposure image recording;
- spectral bandwidth selection.

Usually it consists of the following components (fig.6):

- shutter for cutting out short exposures in the range 0.01 – 0.1 s:
- microscope objectives set to match the speckle size to the pixel size of the detector;
- filter wheel or a diffraction grating monochromator for bandwidth selection;
- atmospheric dispersion compensation prism;
- detector.

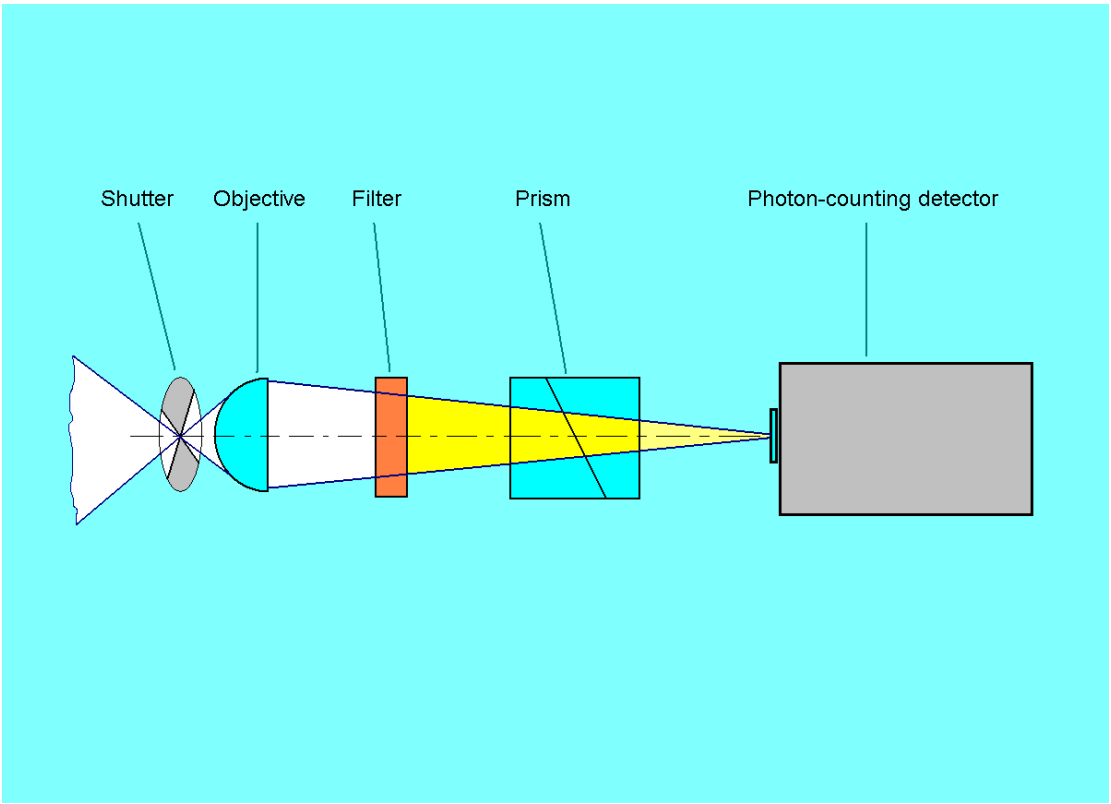

Fig. 6. Speckle camera principal components.

First detectors for speckle interferometry were high-gain image intensifiers optically coupled to film cameras. The sensitivity of such systems was high enough to record speckle images from an object of about 6^{th} magnitude. Later new generation photon counting detectors were applied: intensified CCDs, resistive anode detectors, MAMA and PAPA photon counters. They increased the limiting magnitude of the method to 15^{th} and even 17^{th} mag depending on seeing and the type of an object. For instance, at the BTA 6-m telescope we are still using a 3-stage electrostatic focusing 40 mm cathode image intensifier optically coupled to a fast high-sensitivity CCD camera. The overall quantum efficiency of such detector in the visible region does not exceed few percent, however the photons are recorded with the SNR of the order of 100. In near future, a new generation CCDs with photon counting possibilities, such as EACCD from Marconi, can be used for speckles recording. In the infrared, most of results are obtained with NICMOS-3 and HAWAII arrays.
Photon noise is the most serious problem in speckle image reconstruction technique. It causes the bias that can completely change the result of reconstruction. The photon bias has to be compensated during the reconstruction procedure using the average photon profile determined from the acquisition of photon fields. Photon-counting hole is another problem of photon-counting detectors, connected with their limited dynamic range.

6. Speckle holography

The final output of the Labeyrie's method is the object autocorrelation. For an arbitrary shape object the information cannot be recovered. An exception is the case where a bright point source lies within the isoplanatic path of the object (speckle holography). In this case (see fig. 7) speckle interferometry gives the autocorrelation of the object:

$$AC\,[\,o(x)\,] = \int o(x')\,o(x'+x)\,dx' =$$

$$\int [\,o'(x') + \delta(x'+x_r)]\,[o'(x'+x)) + \delta(x'+x_r+x)]\,dx' =$$

$$\int o'(x')\,o'(x'+x)\,dx' + \int \delta\,(x'+xr)\,\delta\,(x'+x_r+x)\,dx' =$$

$$+ \int o'(x') \, \delta(x' + x_r + x) \, dx' + \int \delta(x' + x_r) \, o'(x' + x) \, dx' =$$

$$= AC[o(x)] + \delta(x) + o(-x - x_r) + o(x - x_r) .$$

Therefore the autocorrelation of $o(x)$ contains two images of the object.

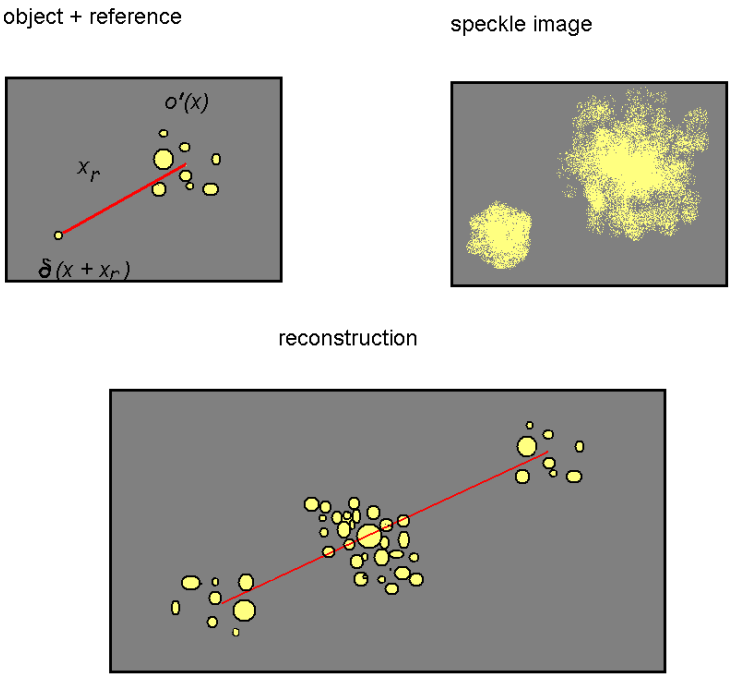

Fig.7. Speckle holography image reconstruction.

Needless to say, astronomical objects are seldom endowed with a point source of high intensity.

7. Shift-and-add algorithm

In this technique each speckle in the blurred image is considered as a distorted image of the object. This follows directly from the simple model of the speckle process resembling a multi-aperture interferometer. The idea of the shift-and-add (SAA) method consists in searching the brightest speckle in each short-exposure image and

shifting whole frames so that the pixels with maximum SNR can be co-added linearly at the same location in the center of the frame (Lynds et al. 1976):

$$i_{SA}(x) = < i_k (x + x_k) > .$$

The instantaneous image of an unresolved star is accepted in this method as

$$i(x) = \Sigma \{ c_k \, \delta(x - x_k) \otimes [f(x) + g_k (x)] \} ,$$

where the crossed circle denotes convolution, $f(x)$ is the normalized ensemble-average speckle profile, $g_k (x)$ describe the normalized differences between the actual speckle profiles and $f(x)$, x_k are the positions of the speckles, and c_k are their weights, proportional to the intensities. An array of impulses is constructed by putting an impulse at each of the speckle gravity center with a weight proportional to the speckle intensity. This impulse array is considered to be an approximation of the short-exposure point-spread function. It is cross-correlated with the speckle frame to recover $f(x)$ and the image of the object. The shift-and-add algorithm is schematically presented in fig.8.

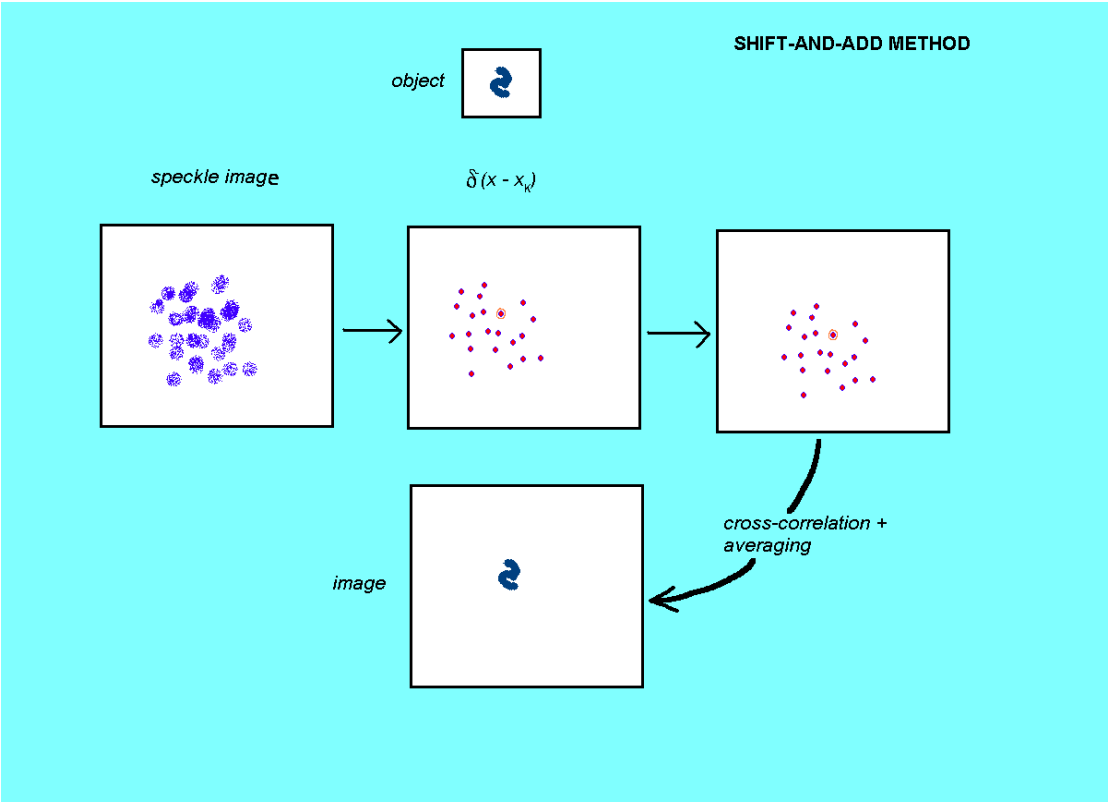

Fig.8. Shift-and-add algorithm presentation.

It is clear that the method can be applied only to bright objects when the photon noise is negligible. Because of numerous possible sources of systematic error in reduction process, it is essential to carefully calibrate $i_{SA}(x)$ with an unresolved point source. Because of these limitations, the shift-and-add method has been seldom used in astronomical practice.

8. Knox-Tompson method of the phase reconstruction

Knox and Tompson (1974) proposed a method for determining the phase of the object transform out to the diffraction limit of the telescope, in order to be able to recover the actual object transform. To extract the phase they proposed to use the statistical autocorrelation of the image transform:

$$< I(u)\, I^*(u + \Delta u) > = O(u)\, O^*(u + \Delta u)\ < S(u)\, S^*(u + \Delta u) > .$$

If the frequency separation is zero, $\Delta u = 0$, eq. is identical to eq. and the phase information is lost. But for a finite $\Delta u < r_0 / \lambda$, the phase information is still present. Knox and Tompson (1974) showed that in case of small Δu, $< S(u)\, S^*(u + \Delta u) >$ has a significant value for all pairs of points along the u-axis op to the diffraction limit of the telescope. Complex correlation $O(u)\, O^*(u + \Delta u)$ in the eq. can be written in the form

$$O(u)\, O^*(u + \Delta u) = |O(u)| \exp(i\varphi(u))\ |O^*(u + \Delta u)| \exp(-i\varphi(u + \Delta u)) .$$

Also

$$\exp(i\varphi(u))\ \exp(-i\varphi(u + \Delta u)) = \exp(-i(\varphi(u) + \varphi(u + \Delta u))) ,$$

which leads to

$$\Delta\varphi(u) \equiv \varphi(u + \Delta u) - \varphi(u),$$

or

$$\varphi(u + \Delta u) = \varphi(u) + \Delta\varphi(u) .$$

This is the recursive equation for calculations of the object Fourier phase. The phase difference between two nearby points of the object Fourier transform can be found from the measurements of the complex correlation between two points in the image Fourier transform. The phase of $O(u)$ at a particular point in the object Fourier plane is then given by the sum of the phase differences from the origin to that point.
The modulus of the object Fourier transform can be found following the classical Labeyrie's procedure. Both the module and the phase give the diffraction-limited image of the object.

9. Speckle masking

As it was shown before, speckle interferometry yields only the diffraction-limited autocorrelation of astronomical objects. Speckle masking (SM) has the additional advantage that it yields diffraction-limited true images (Weigelt 1977; Lohmann et al. 1983). Therefore SM is the solution of the phase problem in speckle interferometry. Below we will briefly outline the principle of the method, following the Weigelt's description.
In SM the same speckle raw data are evaluated as in speckle interferometry:

$$i(x) = o(x) \otimes s(x) .$$

SM processing consists of the 3 steps:
Step 1. Calculation of the ensemble average triple correlation or the ensemble average bispectrum of all speckle interferograms

$$< i_n^{(3)}(x, x') > = < \quad i_n(x'') \, i_n(x'' + x) \, i_n(x'' + x') \, dx'' > ,$$

$$< I_n^{(3)}(u,v) > = < I_n(u) \, I_n(v) \, I_n(-u-v) > .$$

The bispectrum is the Fourier transform of the triple correlation. They both are 4-dimensional functions of coordinates.
Step 2. Inserting $I_n = O \quad S_n$ yields for the average bispectrum

$$< I_n^{(3)}(u,v) > = O(u)\, O(v)\, O(-u-v) \; < S_n(u)\, S_n(v)\, S_n(-u-v) >,$$

where $O(u)\, O(v)\, O(-u-v)$ is the object bispectrum and $< S_n(u)\, S_n(v)\, S_n(-u-v) >$ is called the SM transfer function. This function is greater than zero up to the diffraction cut-off frequency. The SM transfer function is measured in the similar way as the speckle interferometry transfer function.

Step 3. From the object bispectrum $O^{(3)}(u,v)$ the modulus and the phase of the object Fourier transform $O(u)$ can be derived. For the phase reconstruction the recursive algorithm was obtained by Lohmann et al. (1983). Since the four-dimensional bispectrum contains highly redundant information about the two-dimensional Fourier phase of the object, phase recovery is possible in SM with a high SNR. Furthermore, since $< S_n^{(3)}(u,v) >$ is real,

$$\text{phase}\{< I_n^{(3)}(u,v) >\} = \text{phase}\{ O^{(3)}(u,v) \},$$

And therefore, since $< I_n^{(3)}(u,v) >$ can directly serve as raw data for the phase recursion, no transfer function has to be compensated for.

For low light levels a constant and a frequency-dependent photon bias contribute to the bispectrum. In this case a photon bias compensation has to be done to obtain real images.

(Insert Fig.9 “Psi Sgr image reconstruction by speckle masking” – computer presentation).

10. Differential speckle interferometry

Differential speckle interferometry (DSI) is based on the cross-analysis of speckle patterns recorded simultaneously at two or more different wavelengths. The difference between the patterns can be measured independently from the seeing variations. By analogy with long-exposure observations of the colour difference of the coordinates of the star, the differential displacement of speckles can be measured with much higher accuracy than their size. The technique provides a new astrophysical parameter: the vector representing the variation of the of the object photocenter as a function of the wavelength. In the case of objects much smaller than the Airy pattern, DSI makes it possible to measure the difference in the location of the object

photocenter. In another words, DSI measures the displacement between two speckle patterns even when the shift is much smaller than the speckle size. The idea was first published by J.Beckers (1982). He proposed that a pair of two-dimensional speckle images be formed using narrow-band (1A) interference filters and a Wollaston prism in combination with a light chopper. However, taking images simultaneously in different spectral windows entails a serious technical problem, namely, the need for a two-dimensional detector with a very large number of channels. The so-called "*x* - " concept (Petrov & Cuevas 1991) is preferable in terms of technical simplicity and spectral resolution. In this scheme, the speckle image of a star is projected onto a narrow entrance slit of the spectrograph, which transforms each speckle into a separate spectrum. Analysis of spatial information is restricted to only one coordinate along the spectrograph slit. The second coordinate of the detector is used as a spectral axis.

Vector is a function of different parameters therefore its interpretation is not a trivial task. We will illustrate the principles of DSI by its application to binary stars. In this case contains information not only about the relative position of the components in the binary system, but also about their radial velocities, angular diameters and rotation. They all cause the displacement of the relative photocenter of the binary. The intensity ratio between the components changes with the wavelength . If is the separation between the components along the slit, $_1$ is the intensity ratio in the continuum and $_2( )$ is the intensity ratio at the wavelength then the speckle displacement is

$$(_1 - _2) / (1 + _1) (1 + _2) .$$

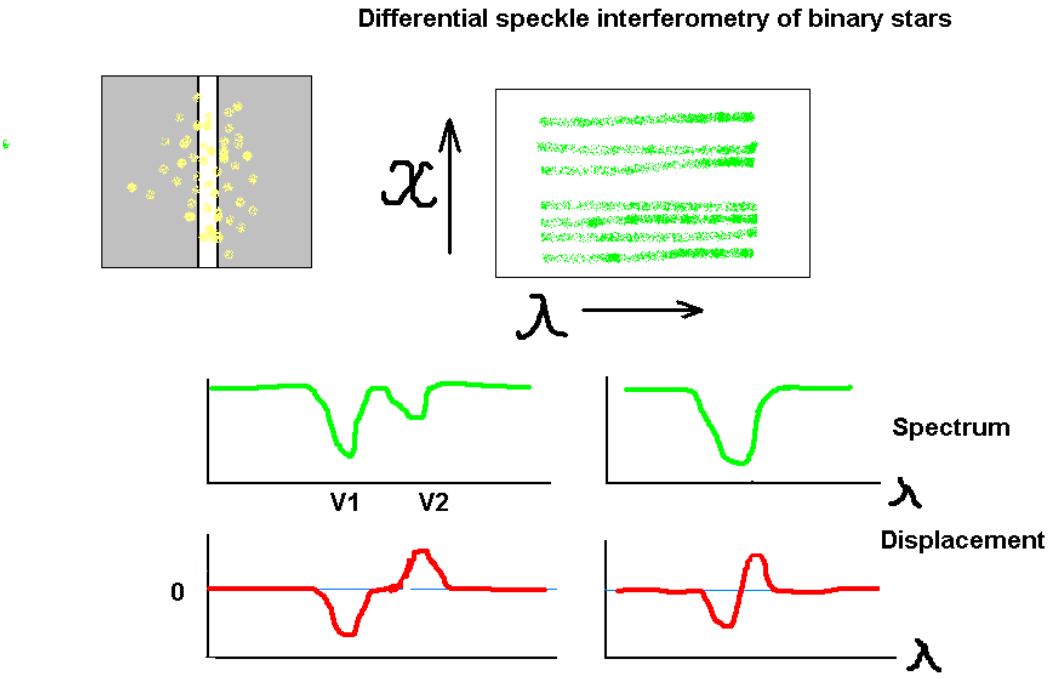

Fig.10. The spectrum and the speckle displacement for a binary star for the "*x*- " experiment.

DSI was applied to recover the individual spectra of the components of Capella. With the 6-m telescope, the 0.001 arcsec error in the measurement, caused by the photon noise, optical aberrations, and geometrical distortions, was achieved.

11. Astronomical applications of speckle interferometry

Speckle interferometry became a productive tool of astrophysics in 80th. The amil fields of application are the following.

Binary star observations: Speckle interferometry revolutionized the field of binary star astrometry. Adding the inclination *i* from the interferometric orbit to the spectroscopic elements allows computation of the component masses, and combining the angular diameter of the orbit with the physical scale set by the spectroscopy yields the distance, or "orbital parallax". To improve the masses speckle orbits must be defined with very high accuracy because the mass-sum is proportional to $sin^3 i$.

Illustrations: 41 Dra and Phi Cyg image reconstructed, binary brown dwarf Gliese 569B.

Measurements of stellar diameters: If the distance to the star is known, its effective temperature is defined by the luminosity and stellar radius. The most direct and model-independent way of measuring effective temperatures is thus the combination of bolometric fluxes with angular diameters. Speckle interferometry gives a possibility to mesure diameters of the nearest and therefore the brightest giants and supergiants like Betelgeuse, Aldebaran and Mira-variables with a formal accuracy about 10%. It should be mentioned that fairly large samples of cooler stars, mostly G, K, and M giants, have also been observed in the visible with the Mk III interferometer with formal errors 1%.

Late type Mira-stars show a wavelength dependence of the photospheric diameter due to the wavelength dependence of the opacity. In essence, interferometry measures the diameter of the = 1 surface, and the atmospheres of cool stars are so tenuous and extended that they become opaque at a substantially larger radius in absorption bands of molecules such as TiO than in the continuum. The very concept of a "photospheric diameter" becomes problematic under these circumstances. Strong variations of diameter with TiO absorption depth have indeed been observed in the Mira variables o Ceti, R Leo, R Cas in qualitative agreement with model predictions. Time series of measurements in well-defined narrow filters covering several pulsation cycles will be required for a more detailed comparison between observations and theory.

Below some examples of such variations are presented for R Cas. In addition, R Cas shows an asymmetric profile in the TiO absorption bands. The variations in the size and position angle of the asymmetric structure occurred on a time scale of a few weeks. Comparison with a small amount of data taken one year earlier at almost the same phases also showed pronounced changes from cycle to cycle.

Measured diameter of the star is systematically larger at 712 nm than at 754 nm. The diameter ratio increases with decreasing effective temperature. The available models do not adequately describe the TiO opacity in the tenuous outer layers of the atmosphere or at the base of the wind; the interferometric data lend support to the existence of an extended "molecular sphere," which has been postulated on the basis of IR spectroscopy. Wavelength-dependent measurements of stellar diameters with spectral resolution across TiO and other molecular bands can thus provide a powerful new tool for the study of the extended atmospheres of cool stars.

Interferometry plays an important role in the controversy about the pulsation mode of Mira variables. The pulsation constant can be determined by combining the period P, angular diameter, and parallax with plausible values for the mass range of Mira stars, and then it can be compared with theoretical values of Q for fundamental-mode or first-overtone pulsations. However many problems remain unclear. Systematic observations with sufficient spectral resolution and coverage, with a range of baseline lengths, and covering the full pulsation cycle will be needed for critical tests of the model atmospheres, and for the eventual determination of the pulsation mode of Mira variables.
Illustrations: Asymmetric image of R Cas.

Disks and shells around the stars at latest stages: Diffraction-limited images of the stars at the latest stages of their evolution were obtained mainly in the 1 – 2 micron range using large monolithic telescopes with an angular resolution up to 50 mas. These images mostly show gaseous nebulae surrounding central objects. In many cases the images are very complex reflecting the complicated multicomponent structure of the circumctellar material. Examples: Red Rectangle with the Keck telescope, dust shell around IRC+10216 from the 6-m telescope.

Young stellar objects: Bispectrum speckle interferometry is employed to explore the immediate environment of deeply embedded young stellar objects. Some reconstructed images show a dynamic range of more than 8 magnitudes thus showing many previously unknown complex structures around young stars. Examples: S140 IRS1 with its multiple outflows.

Extragalactic objects: The input of speckle interferometry in the study of extragalactic object is very modest. The only galaxy that was studied at different observatories, was the nucleus of NGC 1068, the brightest Seyfert galaxy. Illustration: IR image of the nucleus of NGC 1068.

SOME REFERENCES

Beckers, J. 1982 Optica Acta 29 361
Knox, K.T., Thomson, B.J. 1974 ApJ 193 L45
Labeyrie, A. 1970 A&A

Lohmann A. et al. 1983 Applied Optics 22 4028
Petrov, R., Cuevas, S. 1991 Proc. ESO Conf. “High-resolution Imaging by Interferometry II”, Garching, Germany, p.413
Weigelt, G. 1977 Optics Communications 21 55